Published online 16 September 2011 *Nucleic Acids Research, 2012, Vol. 40, No. 2* ***569–580***
doi:10.1093/nar/gkr753

Function and disruption of DNA Methyltransferase 3a cooperative DNA binding and nucleoprotein filament formation

Arumugam Rajavelu[1], Renata Z. Jurkowska[1], Jürgen Fritz[2] and Albert Jeltsch[1,*]

[1]Biochemistry Laboratory and [2]Biophysics Laboratory, School of Engineering and Science, Jacobs University Bremen, Campus Ring 1, 28759 Bremen, Germany

Received June 24, 2011; Revised August 8, 2011; Accepted August 29, 2011

ABSTRACT

The catalytic domain of Dnmt3a cooperatively multimerizes on DNA forming nucleoprotein filaments. Based on modeling, we identified the interface of Dnmt3a complexes binding next to each other on the DNA and disrupted it by charge reversal of critical residues. This prevented cooperative DNA binding and multimerization of Dnmt3a on the DNA, as shown by the loss of cooperative complex formation in electrophoretic mobility shift assay, the loss of cooperativity in DNA binding in solution, the loss of a characteristic 8- to 10-bp periodicity in DNA methylation and direct imaging of protein–DNA complexes by scanning force microscopy. Non-cooperative Dnmt3a-C variants bound DNA well and retained methylation activity, indicating that cooperative DNA binding and multimerization of Dnmt3a on the DNA are not required for activity. However, one non-cooperative variant showed reduced heterochromatic localization in mammalian cells. We propose two roles of Dnmt3a cooperative DNA binding in the cell: (i) either nucleofilament formation could be required for periodic DNA methylation or (ii) favorable interactions between Dnmt3a complexes may be needed for the tight packing of Dnmt3a at heterochromatic regions. The complex interface optimized for tight packing would then promote the cooperative binding of Dnmt3a to naked DNA *in vitro*.

INTRODUCTION

One of the important epigenetic modifications of unicellular and multicellular organisms is DNA methylation. In mammals and other vertebrates, DNA methylation occurs at the C5 position of cytosine bases, mostly at the cytosine residues followed by a guanine (CpG dinucleotides) (1–3). In mammals, DNA methylation has many functions including the control of cellular differentiation and development, the maintenance of chromosomal integrity, parental imprinting, the regulation of gene expression and X-chromosome inactivation. Hypermethylation of tumor-suppressor genes and genome-wide hypomethylation contribute to genomic instability and the development of cancer (4–6). DNA methylation is important for normal cellular differentiation and viability of mammals (3,7), as indicated by the finding that the deletion of any active DNA methyltransferase enzyme in mice is lethal (8,9). Abnormal methylation patterns of genomes are associated with several human diseases, such as Rett syndrome, ICF and Fragile X syndrome. Additionally, DNA methylation plays an important role in brain function (10,11) and changing of DNA methylation patterns is needed for cellular reprogramming (12).

The mammalian DNA methylation machinery consists of the DNA methyltransferase 1 (Dnmt1), which has specificity for hemimethylated DNA and the members of the DNA methyltransferases 3 family, Dnmt3a and Dnmt3b. The Dnmt3 enzymes set up the initial methylation pattern in the genome during embryonic development; however, they also have a role in the preservation of methylation levels at heterochromatin (2,13). The Dnmt3 family also includes one catalytically inactive regulatory factor called DNA methyltransferase 3 like protein (Dnmt3L), which stimulates the activity of *de novo* DNA methyltransferases and assists them at the setting of the initial methylation imprints (14–16). The distinct feature of all Dnmts is that they have a common structure of their C-terminal catalytic domain, which contains 10 amino acids motifs that are conserved among prokaryotic and eukaryotic C5 DNA methyltransferases. Motifs I and X have a role in cofactor binding, motifs IV and VI are involved in catalysis. The conserved region between motifs VIII and IX represents the so called Target Recognition Domain (TDR),

*To whom correspondence should be addressed. Tel: +49 421 200 3247; Fax: +49 421 200 3249; Email: a.jeltsch@jacobs-university.de

which is involved in DNA recognition. The C-terminal domain adopts a fold characteristic for S-adenosyl-L-methionine (AdoMet) dependent methyltransferases (17). Dnmt3a and Dnmt3b have a similar domain arrangement; both contain a variable N-terminal region followed by a PWWP domain, a Cys-rich Zinc-binding ADD domain and the C-terminal catalytic domain (18). The PWWP domain of Dnmt3a reads the H3K36 trimethylation mark (19) and it targets the enzyme to pericentromeric heterochromatin (19–21). The ADD domain of Dnmt3a binds H3 tails unmethylated at K4 (22,23) and stimulates the activity of Dnmt3a after peptide binding (23,24).

The isolated catalytic domain of Dnmt3a (Dnmt3a-C) is catalytically active (25) and it interacts with the C-terminal domain of Dnmt3L (17), forming a butterfly-shaped elongated tetrameric complex (26). This complex contains two monomers of Dnmt3a-C and two monomers of Dnmt3L-C forming a linear 3L–3a–3a–3L heterotetramer. It has two 3a–3L interfaces and one 3a–3a interface. The 3a–3L interaction is mediated by hydrophobic interactions represented by two pairs of phenylalanines F728 and F768 of mouse Dnmt3a and F297 and F337 of mouse Dnmt3L, whereas the 3a–3a interaction is mediated by two charged amino acids R881 and D872 (26). The active sites of the two Dnmt3a are located in the major groove of the DNA in a distance of ~40 Å, such that they could methylate two CG sites separated by ~8–10 bp in one binding event (26,27). In the absence of Dnmt3L, Dnmt3a-C also self-interacts via the FF interface forming reversible oligomers, which bind to more than one DNA molecule oriented in parallel (28). The multimerization of Dnmt3a via the FF and RD interfaces and binding to parallel DNA molecules contribute to the heterochromatic localization of the enzyme. Since Dnmt3L does not possess an RD interface, its binding to Dnmt3a disrupts Dnmt3a oligmerization and leads to the release of Dnmt3a from heterochromatic regions, which could help methylate euchromatic targets like the differential methylated regions in imprinting centers (28).

We have shown previously that the heterotetrameric Dnmt3a/3L complex, as well as oligomeric Dnmt3a-C complexes, bind non-specifically to DNA and cooperatively multimerize on DNA forming large nucleoprotein filaments (26–28). Cooperative multimerization of Dnmt3a/3L and Dnmt3a complexes on DNA was shown by DNA-binding analyses and scanning force microscopy. DNA methylation studies revealed fluctuations of methylation activities along the DNA molecule, which also indicated that there must be a regular arrangement of Dnmt3a complexes on the DNA (26–28). Cooperative DNA binding implies an interaction of Dnmt3a complexes which bind next to each other on the DNA. In this work, based on modeling we have identified one loop that contributes to the interface of such neighboring complexes. By mutating critical residues in the interface and introducing opposite charges, we disrupted the interaction and prevent multimerization of Dnmt3a complexes on DNA, which confirms the predication from modeling. Non cooperative Dnmt3a variants did not lose DNA binding and retained methylation activity, indicating that cooperative DNA binding and multimerization of Dnmt3a on the DNA is not required for enzyme activity. Loss of the cooperative multimerization of Dnmt3a on DNA reduced the heterochromatic localization of the enzyme in NIH3T3 cells, suggesting that it has a role in binding of Dnmt3a to heterochromatic regions.

EXPERIMENTAL PROCEDURES

Site-directed mutagenesis, protein expression and purification

The sequence encoding the C-terminal domain (residues 608–908) of mouse Dnmt3a (Dnmt3a-C) was cloned into pET-28a (Novagen) with an N-terminal His_6-tag (17). Based on modeling, we selected 10 hydrophilic and charged amino acids for the interface study and using the megaprimer site-directed mutagenesis method we mutated these residues to opposite charges to break the interaction (29). Mutagenesis was confirmed by restriction marker analysis and DNA sequencing (Supplementary Figure S1). Protein expression was carried out as described (17). The proteins were purified at high micromolar concentrations using Ni–NTA agarose. Each protein was purified at least twice and the purity of the preparations was estimated to be >95% from Coomassie stained SDS gels (Supplementary Figure S2). The concentrations of the proteins were determined by UV spectrophotometry and confirmed by densitometric analysis of Coomassie stained SDS–polyacrylamide gels. Wild-type like folding of the most important mutants was confirmed by circular dichroism spectroscopy (Supplementary Figure S3).

Methyltransferase activity assay

The methyltransferase activity of Dnmt3a-C wild-type and its interface mutants was measured using biotinylated 30-mer oligonucleotides (Bt-GAG AAG CTG GGA CTT CCG GGA GGA GAG TGC/GCA CTC TCC TCC CGG AAG TCC CAG CTT CTC) containing a single CpG site as described (27). Briefly, DNA methylation was measured by the incorporation of tritiated methyl groups from radioactively labeled AdoMet (Perkin Elmer) into the biotinylated oligonucleotide using the avidin–biotin methylation assay (30). The methylation reactions were carried out in methylation buffer (20 mM HEPES pH 7.2, 1 mM EDTA, 50 mM KCl, 25 μg/ml bovine serum albumin) at 37°C, using 1 μM substrate DNA, 0.76 μM AdoMet and 2 μM Dnmt3a-C wild-type and mutant enzyme. The initial slope of the enzymatic reaction was determined by linear regression. All the kinetic reactions were carried out at least three times. DNA methylation was also measured using a 520-bp DNA fragment containing 40 CpG sites was amplified from phage λ DNA using a biotinylated PCR primer as described (31).

Methylation pattern analysis by bisulfite conversion

DNA methylation patterns of Dnmt3a-C wild-type and mutants were analyzed by hairpin bisulfite analysis (27,32) using an oligonucleotide substrate containing

nine CG sites in an identical sequence context d(AAT TGA CGA CGA CGA CGA CGA CGA CGA CGA CGAC)/d(GAT CGT CGT CGT CGT CGT CGT CGT CGT CGTC). The annealed oligonucleotide (100 nM) was incubated with 2.5 μM enzyme for 2 h in methylation buffer supplemented with 0.32 mM AdoMet (Sigma) at 37°C. The methylation reaction was stopped by freezing the sample in liquid nitrogen, followed by proteinase K digestion (New England Biolabs). Afterwards, the hairpin loop and the adaptors were ligated to the methylated substrates as described (27) and DNA was subjected to bisulfite conversion, cloned into Topo-TA vector (Invitrogen) and individual clones were sequenced essentially as described (33).

In addition, the DNA methylation patterns of Dnmt3a wild-type and mutants was analyzed using a 146-mer DNA substrate amplified from the mammary tumor virus 3′ long-terminal repeat nucleosome A-binding site (34) which contains 10 CpG sites in various distances. Methylation reactions and bisulfite conversion were conducted as described above.

Electrophoretic mobility shift assay

The DNA-binding affinity and cooperativity of Dnmt3a-C and its mutants was analyzed by electrophoretic mobility shift assay (EMSA) carried out essentially as described (27). Briefly, increasing concentrations of Dnmt3a-C wild-type and its interface mutants were incubated with the Cy-5-labeled 146 bp DNA described above (30 nM) in reaction buffer (20 mM HEPES pH 7.5, 1 mM EDTA, 100 mM KCl, 0.5 mg/ml of bovine serum albumin) containing 0.2 mM sinefungin at room temperature for 20 min to form the protein–DNA complex. The protein–DNA complexes were separated on an 8% non-denaturing acrylamide gel, which was scanned with a phosphor imager system (Fuji). Free DNA and wild-type Dnmt3a-C protein were included on the gels as controls.

Fluorescence depolarization

To study equilibrium binding of Dnmt3a to Cy5-labeled oligonucleotide substrates, the change of fluorescence anisotropy caused by protein binding to the DNA was determined using a Cary Eclipse fluorescence spectrophotometer (Varian) equipped with excitation and emission polarizers. Three substrates were used, two 29-mer oligonucleotides (2CG-Cy5 and non-CG-Cy5) and one 60-bp PCR product containing two CpG sites that was amplified from the 146-mer substrate described above (34). All binding substrates were fluorescently (Cy5) labeled at one end.

2CG-Cy5: ACT TGC AA**C** **G**GT CCT AAC **CG**T CAC CTC TT

Non-CG-Cy5: ACT TGC AAC AGT CCT AAC ATT CAC CTC TT

The anisotropy was measured with the excitation wavelength at 633 nm (band-width 10 nm) and the emission wavelength at 665 nm (band-width 10 nm) for 5 s. The reactions were carried out in binding buffer containing 20 mM HEPES pH 7.5, 100 mM KCl, 1 mM EDTA, 2 nM of Cy5-labeled DNA and increasing concentration of protein after incubation at room temperature for 5 min. Each protein concentration was measured in triplicate and the average values were taken for the analysis. Data were least squares fitted using a 1:1 binding model for the 29-mer, where no cooperativity could be detected. For the 60-mer, a cooperative binding model was used determine the dissociation constant (K_D) and Hill coefficient (n) of DNA binding.

Scanning force microscopy

Scanning force microscopy (SFM) experiments were performed with Dnmt3a-C wild-type and the R832E and K837E mutants using a 509-bp DNA fragment, which can be visualized easily in SFM. The DNA was derived from the CG island upstream of the human SUHW1 gene and contains 58 CG sites roughly equally distributed over the entire DNA length. The sample preparation was carried out essentially as described (27). Briefly, the DNA–protein filaments were formed in a reaction volume of 30 μl by incubating 12 nM DNA with 200 nM Dnmt3a-C wild-type or mutants in 50 mM HEPES (pH 7.5), 250 mM NaCl, 1 mM EDTA and 100 μM of sinefungin (Sigma). After addition of DNA to the reaction mixture containing the protein, samples were incubated for 20 min at room temperature to allow for DNA binding. Then, the complex solution (1 μl) was mixed with 9 μl of 5 mM $NiCl_2$ solution and deposited on freshly cleaved mica (Plano, GmbH), allowed to adhere for 2 min and then washed with sterile water. The sample was then dried using compressed air. Protein–DNA filaments were observed by tapping mode in air using a Multimode SFM with a Nanoscope IIIa controller (Veeco Instruments GmbH, Germany) using RTESPW silicon cantilevers (Veeco) with a nominal spring constant of 50 N/m and a resonance frequency of 150 kHz. All images were obtained with a scanning speed of 1 Hz and at a resolution of 512×512 pixels. To remove background slope, raw images were flattened using the Nanoscope software. DNA–protein complexes were considered present if the height of the filament exceeded 150% of the height observed for free DNA molecules and if filaments had an apparent width of at least 20 nm. Filaments were evaluated using the section tool of the Nanoscope V6r12 software and ImageJ software.

Cell culture and laser scanning microscopy

The cellular and sub-nuclear localization of the YFP-fused Dnmt3a and its variants in NIH 3T3 cells was investigated essentially as described (19,28). Briefly, cells were grown in DMEM with 10% (v/v) fetal calf serum and 2 mM L-glutamine at 37°C in 5% (v/v) CO_2. Cells ($1–2 \times 10^5$) were transfected in six-well plates using FuGENE 6 (Roche, Basel, Switzerland; 1 μg total plasmid DNA per well). Transfected NIH3T3 cells were fixed in 4% (w/v) paraformaldehyde. Confocal images were taken using a Carl ZeissLSM510 (Jena, Germany; software version 3.0). The sub-nuclear localization pattern of Dnmt3a was inspected in detail for 100 cells for the wild-type, 25 cells for the R832E and K837E mutants (which did not

differ from wild-type) and 50 cells for the R832E/K837E double mutant and the observed patterns were divided into three categories: spotty, spotty plus diffused and diffused.

RESULTS

We have already shown that Dnmt3a cooperatively multimerizes on DNA. To identify the positions of the individual active sites on the DNA, we employed an 'activity footprint' approach using a substrate which contains nine CG sites next to each other. By applying the hairpin bisulfite technology, the methylation of both strands of individual molecules could be directly studied. After methylation of this substrate with wild-type Dnmt3a-C (Figure 1A) four peaks of preferential methylation were observed, two of them in the lower strand (first peak at sites 7 and 8 and second peak at site 5) and two in the upper strand (first peak at site 5 and second peak at sites 2 and 3). These peaks are all separated by 8- to 10-bp distances both in the same strand and across the strands. This result is in perfect agreement with results of a previous experiment with the Dnmt3a-C/3L-C complex (27). According to the model of the Dnmt3a/3L heterotetramer in complex with DNA (26,27), the methylation of two sites in a distance of 8–10 bp in opposite DNA strands could be attributed to the activity of the active sites from the two central Dnmt3a subunits of the Dnmt3a or Dnmt3a/3L complex, which interact via the RD interface. In contrast, the preferential methylation of sites in distances of 8–10 bp located in the same DNA strand must be due to the presence of two Dnmt3a complexes binding next to each other on the DNA.

The observation of four peaks of methylation suggests that two Dnmt3a-C complexes were bound to the substrate, each of them containing two active centers connected via an RD interface. The right complex methylates the lower strand sites 7 and 8 with one of its active sites and the upper strand site 5 with the other. The left complex approaches the other one and it methylates the lower strand site 5 with one of its active sites and the upper strand sites 2 and 3 with the other (Supplementary Figure S6). The observation that CpG site 5 was preferentially methylated in both DNA strands indicates that the Dnmt3a-C subunits in adjacent Dnmt3a-C complexes can approach each other and interact with both DNA strands of this CpG site.

Several observations support the significance of the methylation peaks at CpG site 5 in both strands: (i) *P*-values are highly significant (except for the comparison of site 5 and 6 in the lower strand where the *P*-value is 0.078) (Supplementary Figure S4), (ii) the geometry of the peaks is palindromic in the upper and lower strand with methylation peaks at sites 2, 3 and 5 in the upper strand corresponding to methylation peaks at sites 8, 7 and 5 in the lower strand, (iii) methylation preferences in opposite strands occur in a distance of 8–10 bp as expected for the two active sites of one Dnmt3a complex (sites 2 and 3 in the upper strand combined with site 5 in the lower strand, site 5 in the upper strand combined with sites 7 and 8 in the lower strand), (iv) a very similar pattern has been observed before in a completely independent experiment (27). The preferred methylation of both DNA strands at site 5 suggests that two Dnmt3a-C subunits from adjacent complexes can simultaneously approach the upper and the

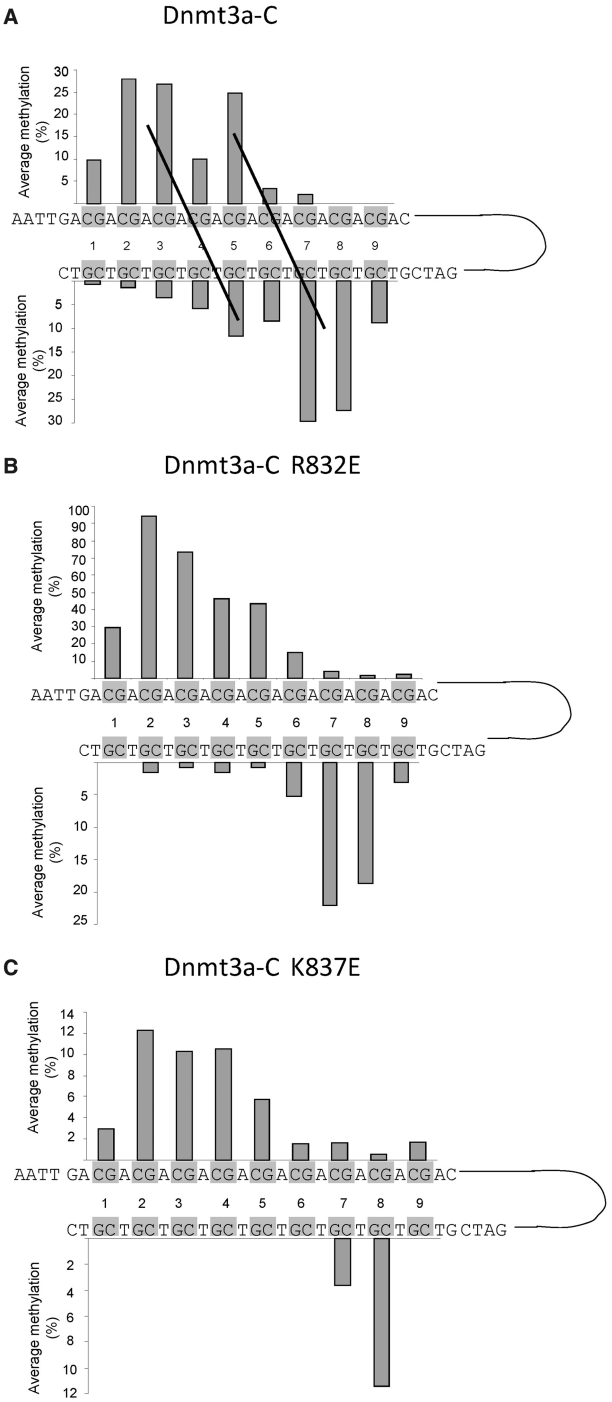

Figure 1. Methylation pattern studied by hairpin bisulfite experiments. Double-stranded hairpin oligonucleotide substrates containing nine equally spaced CG sites were methylated by Dnmt3a-C wild-type or R832E and K837E mutants. 185, 170 and 190 clones were analyzed for Dnmt3a-C wild-type (**A**), R832E (**B**) and K837E (**C**), respectively. The lines in (A) connect peaks of methylation separated by ~8 bp in the opposite DNA strand.

lower strand of one CpG site (site 5 in this case). We took this observation as the starting point for modeling of the multimerization of Dnmt3a-C complexes on DNA.

Modeling of the multimerization of Dnmt3a-C complexes on DNA

To model a complex in which two Dnmt3a-C molecules would interact simultaneously with the upper and lower strand of one CpG site, we have used as a template the structure of the bacterial M.HhaI methyltransferase bound to DNA (35), which was the first methyltransferase for which base flipping could be shown. The complex was used twice and the two DNA strands with the flipped cytosine were annealed with each other to obtain a CpG site with both target cytosines flipped out. Then, Dnmt3a-C molecules were superimposed with the two M.HhaI molecules using the conserved methyltransferase motifs. In the obtained structural model it was also possible to replace each Dnmt3a-C by a Dnmt3a-C/3L-C heterotetramer without larger steric overlaps to obtain a model of two Dnmt3a-C or Dnmt3a-C/3L-C complexes bound to DNA. In this model, two loops (residues 820–855) of the two Dnmt3a-C complexes approach each other symmetrically (Figure 2). This loop is enriched with charged amino acids and may form a hydrophilic interface, which could explain the co-operative multimerization of Dnmt3a-C and Dnmt3a-C/3L-C complexes on DNA. A large part of this loop (residues 827–844) is not ordered in the structure, such that the detailed interactions could not be deduced. The modeling also suggested that the active sites of the two Dnmt3a-C subunits from adjacent complexes that are interacting with the same DNA strand are located ~40 Å apart from each other, indicating that they could methylate two CG sites separated by 10 bp in one binding event. However, given that this modeling did not take into account any conformational changes of the DNA or the Dnmt3a-C complexes, its results need to be interpreted with caution. It was the aim of the following study to investigate if the putative interface suggested by modeling is involved in multimerization of Dnmt3a-C on DNA, if the multimerization can be influenced by mutations and if non-multimerizing Dnmt3a-C variants would still be able to bind and methylate DNA.

DNA binding of Dnmt3a-C and its interface variants studied by EMSAs

To study the role of the selected residues in the cooperative multimerization of Dnmt3a-C, we prepared the putative interface mutants K822E, R827E, R832E,

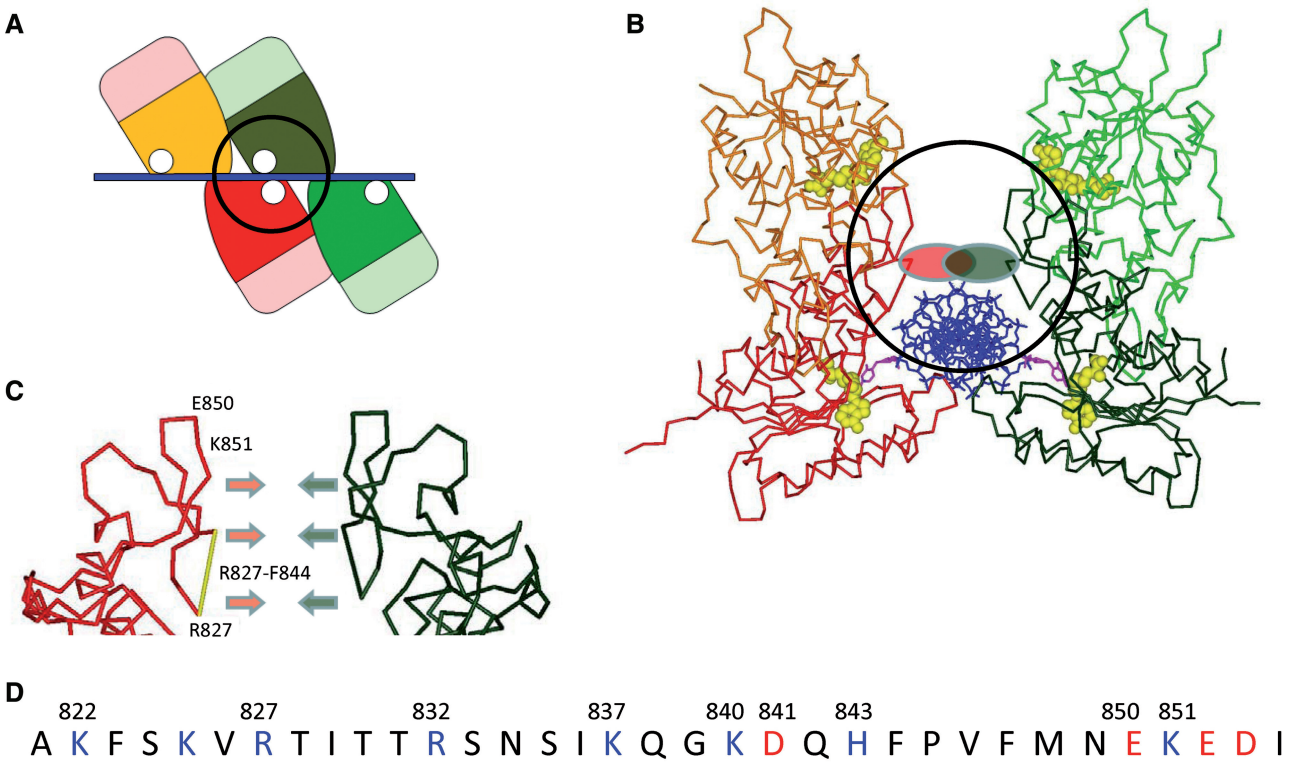

Figure 2. Modeling of two Dnmt3a-C complexes bound to DNA. (**A**) Schematic model of two Dnmt3a-C/3L-C heterotetramers binding next to each other on the DNA, such that a central CpG site could be methylated in both DNA strands. The Dnmt3a-C subunits of the left tetramer are colored orange and red, those of the right tetramer dark green and green. Dnmt3L subunits are colored light red and light green, respectively. (**B**) Model of the central Dnmt3a-C dimers (colored orange and red for one complex and dark green and light green for the other) bound to DNA (blue). The flipped target cytosines are shown in pink, AdoMet is colored yellow. The red and green ovals indicate the proposed interactions of both loops. Note that the amino acids 827–844 are not ordered in the structure and hence not visible in the model. (**C**) Detail of the model showing the interacting loops from the adjacent complexes. The disordered region (amino acids 827–844) is colored yellow. (**D**) Amino acid sequence of the putative interaction loop.

K837E, K840E, D841K, H843E, E850H, K851E and E852K. In each of them, a charged residue was exchanged by a residue carrying an opposite charge. Such exchange should result in a repulsive interaction, if the residue was involved in a charge/charge interaction at the interface and, therefore, disrupt the cooperativity of DNA binding by preventing the binding of two Dnmt3a complexes next to each other. The Dnmt3a-C wild-type and its mutants showed comparable expression in *Escherichia coli* cells. The proteins were purified to similar quality as the wild-type Dnmt3a-C and their folding confirmed by circular dichroism spectroscopy for the R832E and K837E mutants (Supplementary Figure S2 and S3). EMSA were carried out to study the DNA binding of the wild-type Dnmt3a-C and its interface mutants (Figure 3). It had been shown previously that the wild-type Dnmt3a-C multimerizes on the DNA at increasing protein concentration, as indicated by the formation of a protein–DNA complex with very low electrophoretic mobility corresponding to several Dnmt3a-C complexes being bound to the DNA (region 3 in Figure 3) (27). The high degree of cooperativity of the multimerization reaction is indicated by the formation of the multimeric complex without generation of detectable amounts of intermediates. Using identical reaction conditions, the binding of the Dnmt3a-C interface mutants on DNA was studied. The K822E, R832E and K837E mutants shifted the DNA into complexes with an electrophoretic mobility that corresponds to one Dnmt3a-C complex being bound to the DNA (region 2 in Figure 3), which indicates that these variants have lost the ability to multimerize on DNA. The slight differences in the mobilities of these complexes may be explained by the exchanges of charged residues which can affect the behavior of the mutants in native gel systems. DNA binding of these variants is efficient as illustrated by the disappearance of unbound DNA, which indicates that the loss of multimerization is not a trivial effect caused by a reduction of DNA binding. The K840E and K851E mutants bound strongly to DNA and formed large multimeric complexes, but intermediates were also detectable, indicating lower cooperativity of multimerization than observed with the wild-type Dnmt3a-C. E852K showed better DNA binding than the wild-type enzyme and cooperativity could not be evaluated due to the strong binding. The D841K and H843E mutants bound very weakly to the DNA. In summary, we conclude that mutation of most of the candidate residues led to a loss or reduction of the cooperativity of multimerization of Dnmt3a-C complexes on DNA. The most interesting non-multimerizing variants were R832E and K837E, which both completely lost the ability to form cooperative complexes, but showed good DNA binding. To obtain even stronger phenotypic effects, we have also generated and purified the R832E/K837E double mutant and confirmed its folding by circular dichroism spectroscopy (Supplementary Figure S2 and S3). As expected, this variant showed strong DNA binding and loss of multimerization (Figure 3).

DNA binding of Dnmt3a-C and its interface variants studied in solution

To study DNA binding in a homophasic assay, we used Cy5-labeled DNA substrates and determined the increase in fluorescence anisotropy of the Cy5 probe, which accompanied protein binding to the DNA. We first used two 29-mer substrates which either contain two or no

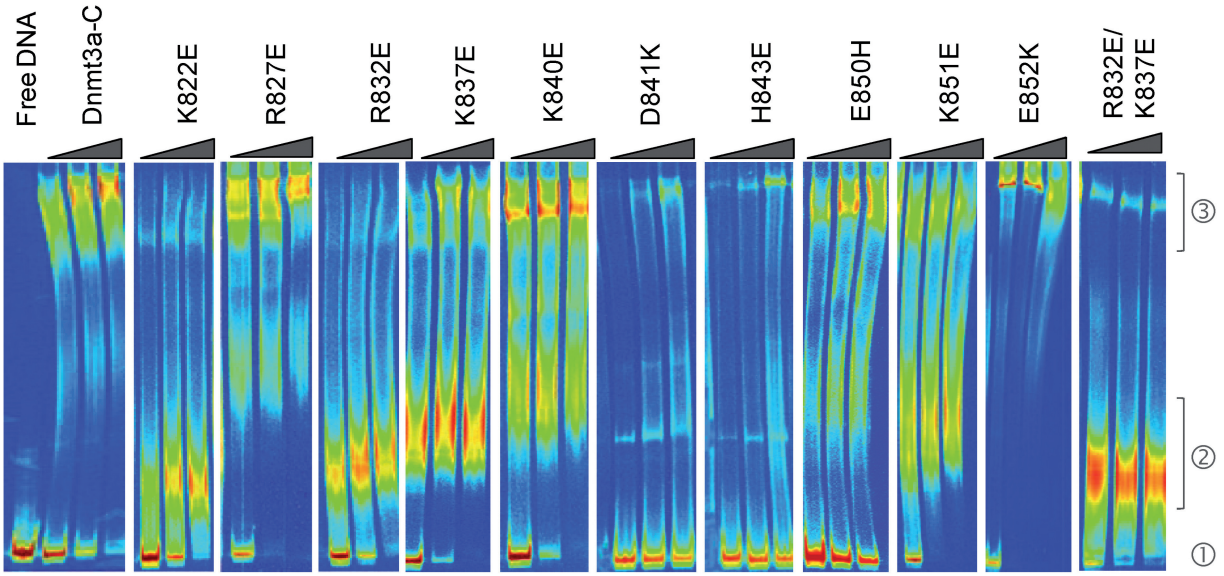

Figure 3. DNA binding and cooperativity studied by EMSA. Dnmt3a-C wild-type protein forms a larger complex with very low electrophoretic mobility (region 3). Free DNA runs in region 1. The K822E, R832E, K837E and R832E/K837E mutants bind to DNA, but form smaller complexes with an electrophoretic mobility that corresponds to one Dnmt3a-C complex being bound to the DNA (region 2). The R827E, K840E, E850H and K851E mutants formed large multimeric complexes, but also some intermediates. The D841K and H843E mutants bound very weakly to the DNA. The E852K mutant showed even better DNA binding than the wild-type enzyme and no change in cooperativity.

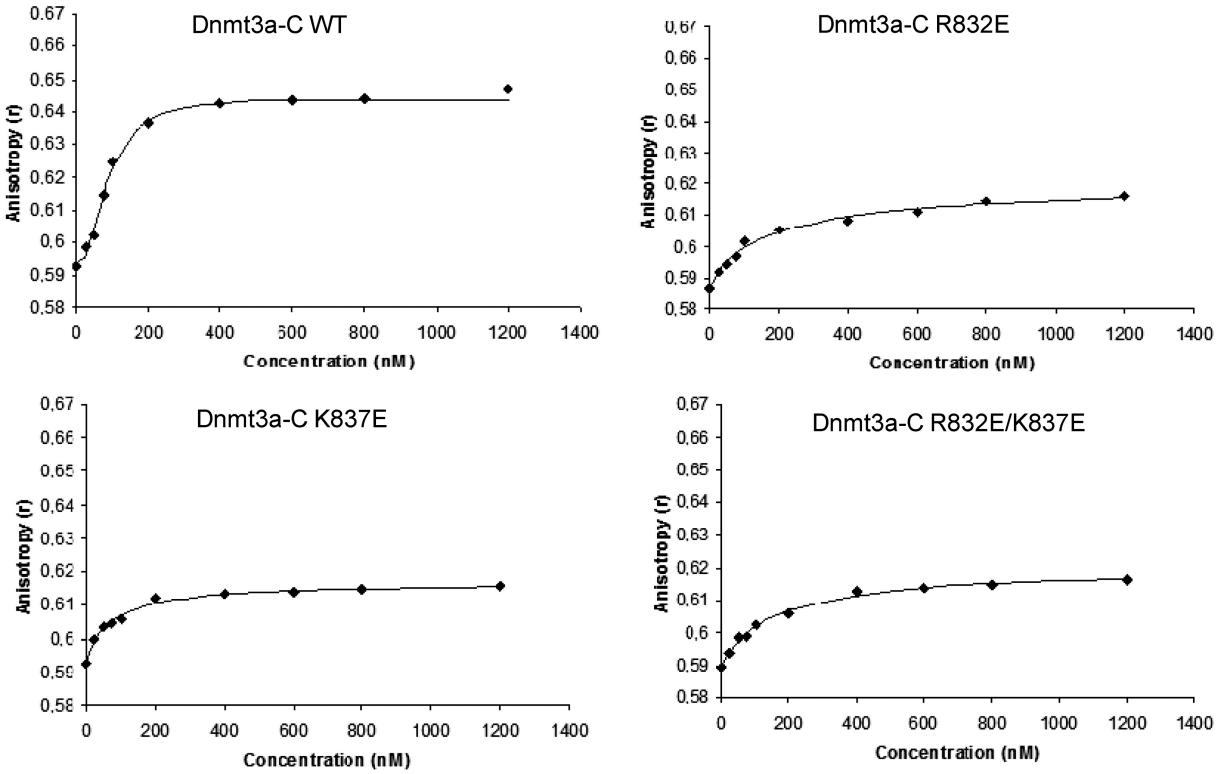

Figure 4. DNA binding and cooperativity studied by fluorescence anisotropy. DNA binding and cooperativity was studies using a 60-mer Cy-5-labeled DNA for the Dnmt3a-C wild-type and R832E, K837E and R832E/K837E proteins at increasing concentration. Dnmt3a-C binds to DNA very strongly with positive cooperativity ($n = 2.2$), suggesting that at least three molecules would bind on the DNA. The R832E, K837E and R832E/K837E mutant proteins showed no cooperativity ($n = 1.0$), but still bound the DNA.

Table 1. Summary for the catalytic activities, DNA-binding constants and DNA-binding cooperativity of wild-type Dnmt3a-C and the interface mutants

Protein	Catalytic activity (% of wild-type)	DNA-binding constant (K_d in nM)	Cooperativity of DNA binding (n)
Dnmt3a-C WT	100	86	2.2
Dnmt3a-C K822E	5	310	1.0
Dnmt3a-C R827E	12	61	2.2
Dnmt3a-C R832E	48	190	1.0
Dnmt3a-C K837E	23	72	1.0
Dnmt3a-C K840E	28	77	1.3
Dnmt3a-C D841K	67	400	1.0
Dnmt3a-C H843E	38	130	1.0
Dnmt3a-C E850H	110	140	1.1
Dnmt3a-C K851E	42	130	1.0
Dnmt3a-C E852K	110	64	1.3
Dnmt3a-C R832E/K837E	5	151	1.0

All values were averages of two or more experiments. Highest standard deviations were ±10% for the catalytic activity, ±25% for the K_d and ±15% for the cooperativity values.

CpG sites. Fluorescence anisotropy was measured in solution containing 2 nM of labeled DNA with increasing protein concentration. Fitting to an equilibrium binding model yielded a K_d of 190 ± 10 nM for the 2-CG substrate and a K_d of 130 ± 12 nM for the non-CG substrate. This result indicated that Dnmt3a-C bound to the DNA without specificity for CpG sites. The slightly better binding to the non-CG substrate might be due to the flanking sequence, which has a strong influence on the DNA interaction and DNA methylation of Dnmt3a that is well documented [see (31) and references therein]. It is also possible that the energy needed for flipping of the target cytosine may reduce the binding to CpG site substrates [see (36) and references therein for examples of prokaryotic DNA methyltransferase studied in this respect].

To investigate cooperative DNA binding of Dnmt3a-C, we used a longer Cy5 labeled 60-mer DNA substrate for subsequent binding studies. The cooperativity of the wild-type Dnmt3a-C and mutant DNA binding was determined by fitting the anisotropy values to the Hill equation. The Dnmt3a-C bound the 60-mer DNA strongly (the calculated K_D value was 86 nM) and the calculated cooperativity value for the wild-type protein was $n = 2.2$, indicating that at least three Dnmt3a-C complexes bound to the DNA in a cooperative manner (Figure 4 and Table 1). Although DNA substrates and assay methods were different, there was a generally nice correspondence between the results of the EMSA and fluorescence polarization DNA-binding studies. In contrast to the wild-type enzyme, the variants that showed loss or reduction of cooperativity in DNA binding in the EMSA, like K822E, R832E, K837E, K851E, or the R832E/K837E double mutant had

cooperativity values close to $n = 1$ (Figure 4 and Table 1). As seen in EMSA, R827E bound DNA with similar affinity and cooperativity as the wild-type and E852K bound DNA better. Also weaker DNA binding by D841K, H843E and E850H was observed. We conclude that R832E, K837E, K851E and the R832E/K837E double mutant are most interesting. All of them show complete loss of cooperativity in DNA binding and their binding affinity is not reduced >50%. K837E is particular striking, because its binding constant is identical to the wild-type Dnmt3a-C (within the limits of error) but cooperativity is completely lost.

Catalytic activity of Dnmt3a-C and its interface variants

The catalytic activity of the variants was determined using an oligonucleotide substrate containing one CpG target site. The K822E, R827E K837E, K840E and H843E mutants showed a strong reduction of methyltransferase activity, whereas R832E, D841K and K851E showed only a weak reduction of activity. The activity of the E850H and E852K mutants was not affected (Figure 5 and Table 1). We tested the activity of the R832E, K837E and R832E/K837E double mutant also using a 520-bp substrate which contains 40 CpG sites and did not observe major differences in the relative activities when compared with wild-type Dnmt3a-C (Supplementary Figure S5). In a previous study, we already investigated the R827A and R832A mutants, which showed 45% and 75% of wild-type activity, respectively (37). The stronger loss of activity observed here can be understood, because the charge reversal done here was expected to cause a stronger effect than the exchange by alanine in the previous study. In summary, the R832E and K851E mutants are most interesting, because both of them show ~50% of activity despite a complete loss of cooperativity in DNA binding, indicating that multimerization is not required for catalytic activity.

Methylation pattern of Dnmt3a-C and its interface variants

We also performed hairpin bisulfite 'activity footprint' experiments with the active non-polymerizing Dnmt3a-C mutants as described above for the wild-type enzyme (Figure 1). The activity footprint of the active non-polymerizing R832E and K837E mutants showed preservation of the preferential methylation of sites 2 and 3 in the upper strand as well as 7 and 8 in the lower strand (Figure 1B and C). However, both mutants showed clear changes in the methylation pattern including a loss of the methylation at CpG site 5 in the lower strand and broadening of the upper strand methylation peak. The methylation of site 5 in the upper strand was still detected (although somehow less prominent). When taken together, these observations suggest that the right Dnmt3a complex is bound to the substrate in the same manner as with the wild-type Dnmt3a-C (Supplementary Figure S6). Upper strand methylation at sites 2, 3 and 4 indicates that the second (left) Dnmt3a-C complex is present as well. The broadening of the methylation peak in the upper strand observed with the mutants suggests that the left complex is more mobile and can reach more sites. This could be due to the loss of the interaction with the right tetramer cased by the mutations (Supplementary Figure S6). Loss of methylation of the lower strand of site 5 suggests that the repulsion caused by the close approximation of two mutations from adjacent complexes led to a conformational change in the lower subunit of the left complex which caused the loss of methylation of the corresponding target site (Supplementary Figure S6). This result indicates that methylation is not possible in both DNA strands at CpG sites in the interface of two Dnmt3a complexes, which is exactly what was expected from our modeling. In addition, the R832E mutant showed a reduced methylation of the lower strand when compared to the upper one. We speculate that the reason for this change is that the mutations affect the flanking sequence preferences of Dnmt3a (upper strand flanking context is ACGA, lower strand it is TCGT). Altered flanking preferences of the mutants were also observed on the larger substrate (see the next paragraph).

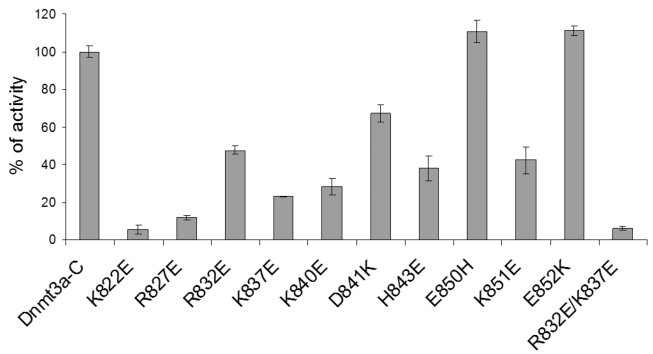

Figure 5. DNA methyltransferase activity of the interface loop mutants. The methyltransferase activity of Dnmt3a-C and its interface mutants was determined using an oligonucleotide substrate containing a single CpG site. All the kinetics were done at least in duplicate. The error bar indicates the standard error of initial slopes.

The DNA methylation patterns of wild-type Dnmt3a-C and the R832E and K837E mutants were also investigated with the 146-bp substrate that was also used for the gel shift experiments. Methylation was analyzed by bisulfite analysis of individual clones to derive the overall methylation profiles, which revealed strong differences between the wild-type and mutant enzymes (Figure 6). However, these overall methylation profiles display the combined effects of the mutations on flanking sequence preferences and preferences for co-methylation in certain distances. Since we were mainly interested in the latter, we focused on those clones showing more than one methylation event and collected the distances of all comethylation events for wild-type and mutants. As shown in the insert of Figure 6, with the wild-type enzyme we observed that 47% of all comethylation events occurred in a distance of 9 or 10 bp (the substrate does not contain CpG sites in a distance of 8 bp). This indicates a strong preference for comethylation in such distances, similarly as shown before with two other DNA substrates (26). This preference was completely lost with the mutants, where only 2% and 8%, respectively, of all comethylation events occurred in this distance range. Since only comethylation events were used for this

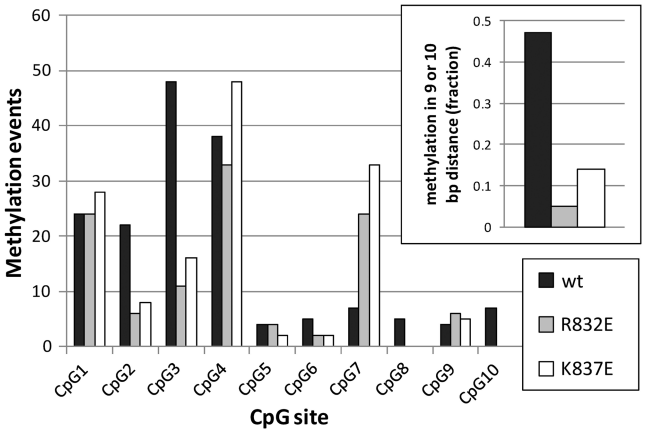

Figure 6. Methylation pattern analysis of wild-type Dnmt3a and its R832E and K837E mutants on the 146-mer DNA substrate which has 10 CpG sites. The insert displays the fraction of co-methylation events in a distance of 9 or 10 bp observed with the wild-type enzyme and the mutants.

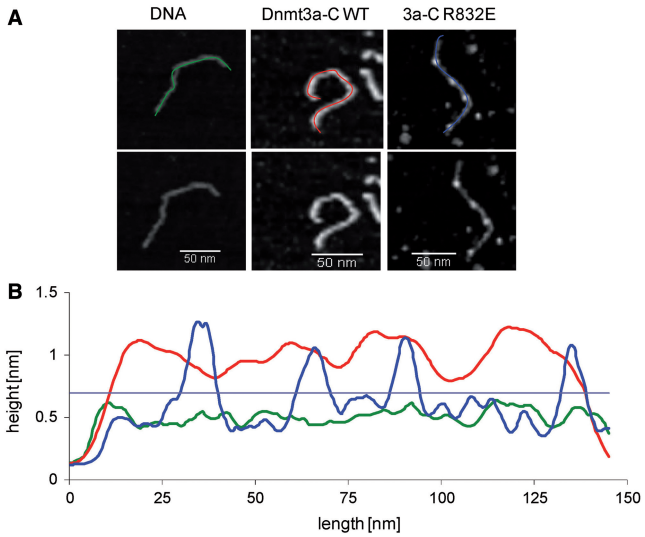

Figure 7. Imaging of Dnmt3a-C/DNA complexes by scanning force microscopy. (**A**) Examples of free DNA, DNA covered with wild-type Dnmt3a-C and DNA with R832E mutant. Wild-type Dnmt3a-C showed complete occupancy of the DNA, whereas the R832E variant showed individual binding events on the DNA. (**B**) Height analysis of protein–DNA complexes. The height for the free DNA is ~0.5 nm, for wild-type Dnmt3a-C a continuous height profile at 1.2 nm is observed, indicative of continuous coverage. In contrast, for the Dnmt3a-C R832E individual binding events with heights of 1.2 nm are separated by free DNA. Additional examples of structures for the R832E and K837E mutants are shown in Supplementary Figure S7A and B.

analysis, this difference cannot be attributed to the lower activity of the mutants. This result confirms our conclusion from the hairpin bisulfite experiment that the preference for co-methylation in a distance of 8–10 bp in the same DNA strand has been lost with the mutants.

Imaging of Dnmt3a-C protein–DNA filaments

We used scanning force microscopy to study the structure of Dnmt3a-C wild-type and R832E and K837E mutant DNA complexes. It had been shown previously (27,28) and was confirmed here that Dnmt3a-C/3L-C heterotetramer and Dnmt3a-C complexes form continuous filamentous structures on DNA, while no binding of individual complexes to the DNA was observed. This result confirms the cooperative DNA binding of Dnmt3a-C. Using the section tool of the SFM software and the ImageJ software, we analyzed the height of the filaments and compared with the height of free DNA molecules for about 100 molecules of free DNA and 60 protein–DNA complexes each for wild-type and the two mutants. With wild-type Dnmt3a-C, we identified many stretches, where the protein continuously occupied the DNA (Figure 7 and Supplementary Figure S7). In contrast, the non-cooperative mutants only showed binding of individual protein complexes to the DNA, as indicated by the sharp and narrow peaks in the height profile (Figure 7, Supplementary Figure S7A and B). Such peaks were never observed with the wild-type enzyme. In contrast, long filamentous structures occupied with protein as seen for the wild-type enzyme were never detected with the R832E and K837E mutants, indicating that the DNA-binding properties of the mutants were radically changed. In conclusion, disruption of the Dnmt3a-C interface of adjacent Dnmt3a-C complexes by introducing opposite charges at key residues prevented the binding of Dnmt3a-C complexes next to each other, leading to the binding of individual complexes on the DNA. This result is in agreement with the EMSA data reported above, which indicated that the R832E and K837E mutants still bind to DNA, but they have lost their cooperativity.

Heterochromatic localization of Dnmt3a variants in NIH 3T3 cells

The N-terminal PWWP domain of Dnmt3a and the multimerization of its catalytic domain are required for the targeting of this enzyme to the heterochromatin (19–21,28). We were interested to determine if the cooperative DNA binding of Dnmt3a also has an influence on its heterochromatic localization. Hence, we have carried out localization studies with variants that lost cooperative DNA binding. Consistent with previous studies, wild-type Dnmt3a localized exclusively to multiple heterochromatic spots in NIH3T3 cells (19–21,28). Despite their loss of the cooperative DNA binding, the R832E and K837E variants showed a similar localization pattern as the wild-type protein (Figure 8A and C). However, the R832E/K837E double mutant showed an altered sub-nuclear localization pattern with many cells showing a diffused nuclear localization that was never observed with wild-type Dnmt3a (Figure 8B and C). This result indicates that the two mutations in the R832E/K837E double mutant protein prevent the approximation of adjacent Dnmt3a complexes, which interferes with heterochromatic localization of the enzyme. This observation suggests that Dnmt3a binds to heterochromatin by forming close contacts between adjacent Dnmt3a complexes.

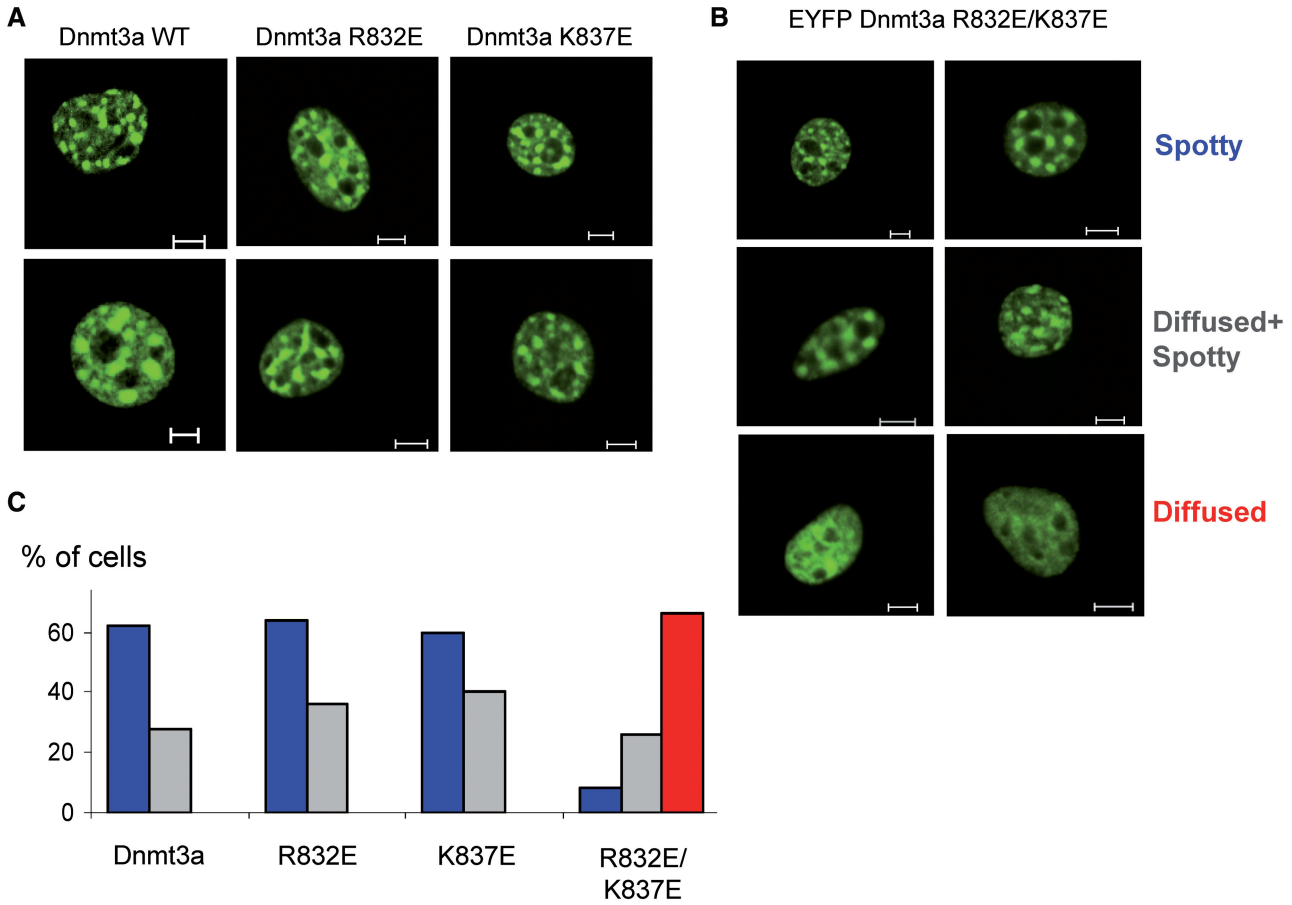

Figure 8. Localization of Dnmt3a in NIH 3T3 cells. (**A**) Localization of the eYFP-tagged full-length Dnmt3a wild-type and R832E and K837E mutants in NIH 3T3 cells. The wild-type protein and single mutants show localization to heterochromatic spots (19,28). (**B**) Localization of the YFP-tagged full-length Dnmt3a R832E/K837E double mutant in NIH 3T3 cells, showing three different patterns of nuclear localization: diffuse, spotty plus diffuse and spotty. (**C**) Quantification of the localizations patterns observed with wild-type Dnmt3a and the R832E/K837E mutant protein. The scale bars represent 5 μm.

DISCUSSION

Crystallographic studies revealed that the C-terminal domain of Dnmt3L interacts with Dnmt3a-C and forms a butterfly-shaped elongated tetrameric complex (26,27). The active sites of the two Dnmt3a are located in the major groove of DNA ~40-Å apart from each other and methylate two CG sites separated by 8–10 bp in one binding event (26,27). In the absence of Dnmt3L, Dnmt3a-C also interacts via the FF interface forming reversible oligomers, which bind to more than one DNA molecule oriented in parallel (28). In the cell, Dnmt3a is tightly bound to heterochromatin (2,13), as demonstrated by the observation that it can only be eluted from the chromatin by treatment with high salt (38,39). This stable binding requires the interaction of the PWWP domain with H3K36me3 (19) as well as oligomerization of Dnmt3a and binding to parallel DNA molecules (28). The oligomerization of Dnmt3a is disrupted by Dnmt3L, which redistributes the enzyme for methylation of euchromatic targets (28).

In our previous studies, we showed cooperative DNA binding of Dnmt3a-C and Dnmt3a-C/3L-C complexes (26,27). The cooperative multimerization of proteins on DNA is based on two features, a relatively non-specific DNA binding and a favorable interaction between adjacent protein molecules. Dnmt3a-C indeed binds non-specifically to DNA, such that the first of the pre-conditions for cooperative DNA binding is fulfilled. Here, we have identified the putative interface between Dnmt3a-C complexes bound next to each other on the DNA by modeling and disrupted the interaction by introducing opposite charges at key residues. The mutants retained DNA binding and residual catalytic activity, but lost cooperativity in DNA binding, indicating that we have successfully mapped the oligomerization interface. The interacting loops are partially disordered in the Dnmt3a-C/Dnmt3L-C structure (26), which might be due to the absence of a second enzyme tetramer bound to the DNA. The successful modeling of the interface and its targeted disruption illustrates the good level of understanding we have reached for this important enzyme and its complicated quaternary structure.

Ever since its first observation, the cooperative multimerization of Dnmt3a-C on the DNA was

considered puzzling, because it was difficult to attribute a biological function to this '*in vitro*' property. Is there enough naked DNA available in the cell nucleus to allow for the formation of long protein nucleofilaments? What could be the role of the cooperativity in DNA binding? In this study, we reconfirmed the cooperative DNA binding of Dnmt3a-C by employing an EMSA, showing the cooperativity of DNA binding in solution, confirming a characteristic 8- to 10-bp periodicity in DNA methylation in the same DNA strand and direct imaging of protein–DNA complexes by scanning force microscopy. We prepared non-cooperative variants which lost all these properties giving further credence to the experimental approaches. At the same time the non-cooperative mutants did not lose DNA binding and retained methylation activity, which indicates that cooperative DNA binding and multimerization of Dnmt3a on the DNA are not required for enzyme activity—a conclusion that further emphasizes the question of the physiological role of this entire process.

We could imagine two models for the role of cooperative multimerization of Dnmt3a complexes on DNA in cells. One possible interpretation is based on the observation that the formation of a defined structured nucleoprotein complex of Dnmt3a on DNA leads to a characteristic methylation pattern with peaks in a distance of 8–10 bp on the DNA (Figures 5A and 6) (27). Such patterns have been observed in genome-wide DNA methylation analyses (33,40,41) and a similar periodicity of presentation of CpG sites has been found in imprinted Dnmt3a/3L target sites (26), suggesting that they may be of importance. We show here that Dnmt3a-C variants which lost cooperative complex formation did not generate such defined patterns. Hence, multimerization of Dnmt3a and stable filament formation is needed for periodic methylation of DNA. Such binding and periodic DNA methylation could be possible in linker DNA regions or after chromatin remodeling. However, since the 8–10 bp periodicity coincides with the helical repeat length of DNA, it is still unclear if it contains epigenetic information or just reflects the accessibility of CpG sites when the DNA is bound to nucleosomes.

An alternative model is based on the finding that Dnmt3a-C is known to bind very tightly to heterochromatic sites. We have provided evidence that the interaction of the PWWP domain with H3K36me3 is essential for this localization (19), but also the oligomerization of the Dnmt3a protein together with its ability of binding to several DNA molecules oriented in parallel is required (28). We show here that the disruption of the interface of Dnmt3a complexes that is needed for the side by side binding on the DNA, also leads to a disruption of heterochromatic targeting of the enzyme. What emerges is a picture of Dnmt3a binding to very DNA dense regions, which have a condensed and regular structure. We propose that the tight packing of Dnmt3a at these regions requires the close approximation of adjacent Dnmt3a complexes bound to the same DNA molecule. The mutations in the R832E/K837E double mutant protein interfere with such approximation, which could explain the weakening of the heterochromatic localization. In this model, the tight packing of Dnmt3a at heterochromatic DNA regions is important for the physiology of this enzyme. Tight packing of the enzyme directly requires some favorable interactions between adjacent complexes, which will automatically result in a cooperative binding of the complexes to DNA in an *in vitro* assay, if the general DNA binding is non-specific. Hence, the cooperative binding to naked DNA *in vitro* could be a consequence of the optimization of the interface of Dnmt3a complexes for tight packing of Dnmt3a at heterochromatic regions *in vivo* and not a property directly selected for during molecular evolution of Dnmt3a.

SUPPLEMENTARY DATA

Supplementary Data are available at NAR Online.

ACKNOWLEDGEMENTS

Thanks are due to Dr Nils Anspach for help with the SFM analyses.

FUNDING

Funding for open access charge: Deutsche Forschungsgemeinschaft (JE 252/10-1).

Conflict of interest statement. None declared.

REFERENCES

1. Cheng,X. and Blumenthal,R.M. (2010) Coordinated chromatin control: structural and functional linkage of DNA and histone methylation. *Biochemistry*, **49**, 2999–3008.
2. Jurkowska,R.Z., Jurkowski,T.P. and Jeltsch,A. (2011) Structure and function of mammalian DNA methyltransferases. *Chembiochem*, **12**, 206–222.
3. Kim,J.K., Samaranayake,M. and Pradhan,S. (2009) Epigenetic mechanisms in mammals. *Cell Mol. Life Sci.*, **66**, 596–612.
4. Feinberg,A.P. and Tycko,B. (2004) The history of cancer epigenetics. *Nat. Rev. Cancer*, **4**, 143–153.
5. Jones,P.A. and Baylin,S.B. (2007) The epigenomics of cancer. *Cell*, **128**, 683–692.
6. Berdasco,M. and Esteller,M. (2010) Aberrant epigenetic landscape in cancer: how cellular identity goes awry. *Dev. Cell*, **19**, 698–711.
7. Meissner,A. (2010) Epigenetic modifications in pluripotent and differentiated cells. *Nat. Biotechnol.*, **28**, 1079–1088.
8. Li,E., Bestor,T.H. and Jaenisch,R. (1992) Targeted mutation of the DNA methyltransferase gene results in embryonic lethality. *Cell*, **69**, 915–926.
9. Okano,M., Bell,D.W., Haber,D.A. and Li,E. (1999) DNA methyltransferases Dnmt3a and Dnmt3b are essential for de novo methylation and mammalian development. *Cell*, **99**, 247–257.
10. Feinberg,A.P. (2007) Phenotypic plasticity and the epigenetics of human disease. *Nature*, **447**, 433–440.
11. Meaney,M.J. and Ferguson-Smith,A.C. (2010) Epigenetic regulation of the neural transcriptome: the meaning of the marks. *Nat. Neurosci.*, **13**, 1313–1318.
12. De Carvalho,D.D., You,J.S. and Jones,P.A. (2010) DNA methylation and cellular reprogramming. *Trends Cell. Biol.*, **20**, 609–617.
13. Jones,P.A. and Liang,G. (2009) Rethinking how DNA methylation patterns are maintained. *Nat. Rev. Genet.*, **10**, 805–811.
14. Bourc'his,D., Xu,G.L., Lin,C.S., Bollman,B. and Bestor,T.H. (2001) Dnmt3L and the establishment of maternal genomic imprints. *Science*, **294**, 2536–2539.

15. Hata,K., Okano,M., Lei,H. and Li,E. (2002) Dnmt3L cooperates with the Dnmt3 family of de novo DNA methyltransferases to establish maternal imprints in mice. *Development*, **129**, 1983–1993.
16. Bourc'his,D. and Bestor,T.H. (2004) Meiotic catastrophe and retrotransposon reactivation in male germ cells lacking Dnmt3L. *Nature*, **431**, 96–99.
17. Gowher,H., Liebert,K., Hermann,A., Xu,G. and Jeltsch,A. (2005) Mechanism of stimulation of catalytic activity of Dnmt3A and Dnmt3B DNA-(cytosine-C5)-methyltransferases by Dnmt3L. *J. Biol. Chem.*, **280**, 13341–13348.
18. Cheng,X. and Blumenthal,R.M. (2008) Mammalian DNA methyltransferases: a structural perspective. *Structure*, **16**, 341–350.
19. Dhayalan,A., Rajavelu,A., Rathert,P., Tamas,R., Jurkowska,R.Z., Ragozin,S. and Jeltsch,A. (2010) The Dnmt3a PWWP domain reads histone 3 lysine 36 trimethylation and guides DNA methylation. *J. Biol. Chem.*, **285**, 26114–26120.
20. Chen,T., Tsujimoto,N. and Li,E. (2004) The PWWP domain of Dnmt3a and Dnmt3b is required for directing DNA methylation to the major satellite repeats at pericentric heterochromatin. *Mol. Cell Biol.*, **24**, 9048–9058.
21. Ge,Y.Z., Pu,M.T., Gowher,H., Wu,H.P., Ding,J.P., Jeltsch,A. and Xu,G.L. (2004) Chromatin targeting of de novo DNA methyltransferases by the PWWP domain. *J. Biol. Chem.*, **279**, 25447–25454.
22. Otani,J., Nankumo,T., Arita,K., Inamoto,S., Ariyoshi,M. and Shirakawa,M. (2009) Structural basis for recognition of H3K4 methylation status by the DNA methyltransferase 3A ATRX-DNMT3-DNMT3L domain. *EMBO Rep.*, **10**, 1235–1241.
23. Zhang,Y., Jurkowska,R., Soeroes,S., Rajavelu,A., Dhayalan,A., Bock,I., Rathert,P., Brandt,O., Reinhardt,R., Fischle,W. *et al.* (2010) Chromatin methylation activity of Dnmt3a and Dnmt3a/3L is guided by interaction of the ADD domain with the histone H3 tail. *Nucleic Acids Res.*, **38**, 4246–4253.
24. Li,B.Z., Huang,Z., Cui,Q.Y., Song,X.H., Du,L., Jeltsch,A., Chen,P., Li,G., Li,E. and Xu,G.L. (2011) Histone tails regulate DNA methylation by allosterically activating de novo methyltransferase. *Cell Res.*, **21**, 1172–1181.
25. Gowher,H. and Jeltsch,A. (2002) Molecular enzymology of the catalytic domains of the Dnmt3a and Dnmt3b DNA methyltransferases. *J. Biol. Chem.*, **277**, 20409–20414.
26. Jia,D., Jurkowska,R.Z., Zhang,X., Jeltsch,A. and Cheng,X. (2007) Structure of Dnmt3a bound to Dnmt3L suggests a model for de novo DNA methylation. *Nature*, **449**, 248–251.
27. Jurkowska,R.Z., Anspach,N., Urbanke,C., Jia,D., Reinhardt,R., Nellen,W., Cheng,X. and Jeltsch,A. (2008) Formation of nucleoprotein filaments by mammalian DNA methyltransferase Dnmt3a in complex with regulator Dnmt3L. *Nucleic Acids Res.*, **36**, 6656–6663.
28. Jurkowska,R.Z., Rajavelu,A., Anspach,N., Urbanke,C., Jankevicius,G., Ragozin,S., Nellen,W. and Jeltsch,A. (2011) Oligomerization and binding of the DNMT3A DNA methyltransferase to parallel DNA molecules, heterochromatic localization and role of DNMT3L. *J. Biol. Chem.*, **286**, 24200–24207.
29. Jeltsch,A. and Lanio,T. (2002) Site-directed mutagenesis by polymerase chain reaction. *Methods Mol. Biol.*, **182**, 85–94.
30. Roth,M. and Jeltsch,A. (2000) Biotin-avidin microplate assay for the quantitative analysis of enzymatic methylation of DNA by DNA methyltransferases. *Biol. Chem.*, **381**, 269–272.
31. Jurkowska,R.Z., Siddique,A.N., Jurkowski,T.P. and Jeltsch,A. (2011) Approaches to enzyme and substrate design of the murine Dnmt3a DNA methyltransferase. *Chembiochem*, **12**, 1589–1594.
32. Laird,C.D., Pleasant,N.D., Clark,A.D., Sneeden,J.L., Hassan,K.M., Manley,N.C., Vary,J.C. Jr, Morgan,T., Hansen,R.S. and Stoger,R. (2004) Hairpin-bisulfite PCR: assessing epigenetic methylation patterns on complementary strands of individual DNA molecules. *Proc. Natl Acad. Sci. USA*, **101**, 204–209.
33. Zhang,Y., Rohde,C., Tierling,S., Jurkowski,T.P., Bock,C., Santacruz,D., Ragozin,S., Reinhardt,R., Groth,M., Walter,J. *et al.* (2009) DNA methylation analysis of chromosome 21 gene promoters at single base pair and single allele resolution. *PLoS Genet.*, **5**, e1000438.
34. Flaus,A. and Richmond,T.J. (1998) Positioning and stability of nucleosomes on MMTV 3′LTR sequences. *J. Mol. Biol.*, **275**, 427–441.
35. Klimasauskas,S., Kumar,S., Roberts,R.J. and Cheng,X. (1994) HhaI methyltransferase flips its target base out of the DNA helix. *Cell*, **76**, 357–369.
36. Jeltsch,A., Roth,M. and Friedrich,T. (1999) Mutational analysis of target base flipping by the EcoRV adenine-N6 DNA methyltransferase. *J. Mol. Biol.*, **285**, 1121–1130.
37. Gowher,H., Loutchanwoot,P., Vorobjeva,O., Handa,V., Jurkowska,R.Z., Jurkowski,T.P. and Jeltsch,A. (2006) Mutational analysis of the catalytic domain of the murine Dnmt3a DNA-(cytosine C5)-methyltransferase. *J. Mol. Biol.*, **357**, 928–941.
38. Jeong,S., Liang,G., Sharma,S., Lin,J.C., Choi,S.H., Han,H., Yoo,C.B., Egger,G., Yang,A.S. and Jones,P.A. (2009) Selective anchoring of DNA methyltransferases 3A and 3B to nucleosomes containing methylated DNA. *Mol. Cell Biol.*, **29**, 5366–5376.
39. Sharma,S., De Carvalho,D.D., Jeong,S., Jones,P.A. and Liang,G. (2011) Nucleosomes containing methylated DNA stabilize DNA methyltransferases 3A/3B and ensure faithful epigenetic inheritance. *PLoS Genet.*, **7**, e1001286.
40. Zhang,X., Yazaki,J., Sundaresan,A., Cokus,S., Chan,S.W., Chen,H., Henderson,I.R., Shinn,P., Pellegrini,M., Jacobsen,S.E. *et al.* (2006) Genome-wide high-resolution mapping and functional analysis of DNA methylation in arabidopsis. *Cell*, **126**, 1189–1201.
41. Chodavarapu,R.K., Feng,S., Bernatavichute,Y.V., Chen,P.Y., Stroud,H., Yu,Y., Hetzel,J.A., Kuo,F., Kim,J., Cokus,S.J. *et al.* (2010) Relationship between nucleosome positioning and DNA methylation. *Nature*, **466**, 388–392.